Constraining First-Order Phase Transitions with Curvature Perturbations

Jing Liu,[1,2,3,*] Ligong Bian,[4,5,†] Rong-Gen Cai,[6,7,3,‡] Zong-Kuan Guo,[6,7,3,§] and Shao-Jiang Wang[6,‖]

[1]International Centre for Theoretical Physics Asia-Pacific, University of Chinese Academy of Sciences, 100190 Beijing, China
[2]Taiji Laboratory for Gravitational Wave Universe, University of Chinese Academy of Sciences, 100049 Beijing, China
[3]School of Fundamental Physics and Mathematical Sciences, Hangzhou Institute for Advanced Study, University of Chinese Academy of Sciences, Hangzhou 310024, China
[4]Department of Physics and Chongqing Key Laboratory for Strongly Coupled Physics, Chongqing University, Chongqing 401331, People's Republic of China
[5]Center for High Energy Physics, Peking University, Beijing 100871, China
[6]CAS Key Laboratory of Theoretical Physics, Institute of Theoretical Physics, Chinese Academy of Sciences, P.O. Box 2735, Beijing 100190, China
[7]School of Physical Sciences, University of Chinese Academy of Sciences, No.19A Yuquan Road, Beijing 100049, China

(Received 26 September 2022; revised 12 December 2022; accepted 11 January 2023; published 31 January 2023)

The randomness of the quantum tunneling process induces superhorizon curvature perturbations during cosmological first-order phase transitions. We for the first time utilize curvature perturbations to constrain the phase transition parameters, and find that the observations of the cosmic microwave background spectrum distortion and the ultracompact minihalo abundance can give strict constraints on the phase transitions below 100 GeV, especially for the low-scale phase transitions and some electroweak phase transitions. The current constraints on the phase transition parameters are largely extended by the results of this work, therefore provide an novel approach to probe related new physics.

DOI: 10.1103/PhysRevLett.130.051001

Introduction.—The cosmological first-order phase transitions (PTs) are expected to take place in many well-motivated new physics models [1–4]. During a first-order PT, at least two nondegenerated local minima simultaneously appear, and the metastable phase decays due to quantum tunneling or thermal fluctuations [5–8]. True vacuum bubbles copiously nucleate and then expand until they collide with each other, releasing the vacuum energy into bubble walls and background plasma. As violent processes in the early Universe, the PTs are expected to produce observable relics including gravitational waves (GWs) [9,10], primordial magnetic fields [11–13] and baryon asymmetry [14]. Since the electroweak PT in the standard model of particle physics is crossover [15], the experiments aiming at observing the relics of the first-order PTs help to determine or constrain the parameters of new physics models. Observing gravitational waves produced during the PTs is one of the main scientific goals of various observational projects, such as LISA [16], *Taiji* [17], TianQin [18], aLIGO [19], and SKA [20]. The corresponding constraints from the upper bound of stochastic GW backgrounds can be found in Ref. [21] (NANOGrav), Ref. [22] (PPTA), and Ref. [23] (LIGO-Virgo).

We find that the randomness of the quantum tunneling process during the PTs can induce curvature perturbations both outside and inside the Hubble horizon, which can be orders of magnitude larger than primordial perturbations from inflation [24]. The asynchronism of vacuum decay affects the averaged equation of state within different Hubble horizons during the PTs, then induces curvature perturbations at superhorizon scales after the PTs. This kind of curvature perturbations is independent of that produced from quantum fluctuations during inflation. The idea of inducing curvature perturbations from PTs was proposed in the 1980s [25–30] and the case $\beta/H_* \lesssim \mathcal{O}(1)$ is ruled out. Except the cosmic microwave background (CMB) observations [31], the current limits of the cosmic microwave background spectral distortions, the helium abundance, and the ultracompact minihalo (UCMH) abundance give constraints on curvature perturbations for $1\ \mathrm{Mpc}^{-1} < k < 10^7\ \mathrm{Mpc}^{-1}$, which allow us to constrain the PTs that happen at energy scales up to 100 GeV, such as QCD phase transitions with a large neutrino chemical potential [32], dark phase transitions predicted in some composite dark matter models, strongly interacting massive particle dark matter models, and Twin Higgs models, etc. [33], and some electroweak PTs motivated for the baryon asymmetry and dark matter [34–37]. These upper bounds on $\mathcal{P}_\mathcal{R}$ are used to be employed to constrain the inflationary models and the primordial black hole abundance [38,39]. In this Letter, we for the first time utilize upper bounds on $\mathcal{P}_\mathcal{R}$ to constrain the PT parameters through induced curvature perturbations, which largely extends the current constraints from the mostly discussed GWs from bubble collisions and sound waves. For convenience, we choose $c = 8\pi G = 1$ throughout this Letter.

Curvature perturbations induced from the PTs.—The nucleation rate of true vacuum bubbles generally takes the exponential form [5,40]

$$\Gamma(t) = \Gamma_0 e^{\beta t}, \tag{1}$$

where Γ_0 and β are approximately constants. For fast PTs, β^{-1} is also an estimation of the PT duration time. The averaged probability of the false vacuum, $F(t)$, reads [29]

$$F(t) = \exp\left[-\frac{4\pi}{3}\int_{t_i}^{t} dt' \Gamma(t') a^3(t') r^3(t,t')\right], \tag{2}$$

where t_i is the time when quantum tunneling starts and $r(t,t') \equiv \int_{t'}^{t} a^{-1}(\tau) d\tau$ is the comoving radius of true vacuum bubbles. Before t_i, the field settles in the false vacuum so that $F(t < t_i) = 1$. After t_i, $F(t)$ decreases since the vacuum energy transfers into bubble walls and background plasma. The PT temperature T_* is evaluated at the percolation time t_p where $F(t_p) = 0.7$. The Friedmann equation and the equations of motion read

$$H^2 = \frac{1}{3}(\rho_r + \rho_w + \rho_v), \tag{3}$$

$$\rho_v = F(t)\Delta V, \tag{4}$$

$$\frac{d(\rho_r + \rho_w)}{dt} + 4H(\rho_r + \rho_w) = \left(-\frac{d\rho_v}{dt}\right), \tag{5}$$

where H is the Hubble parameter, ρ_r, ρ_w, and ρ_v are the energy densities of background radiation, bubble walls, and the false vacuum, respectively. ΔV is the energy density difference between the false and true vacua. In Eq. (5) we assume the bubble wall velocity is close to 1 so that bubble walls and the background plasma are both ultrarelativistic. The left-hand side of Eq. (5) represents the evolution of bubble walls and background plasma in the expanding Universe and the right-hand side results from the decay of the vacuum energy.

Since in the expanding Universe ρ_r and ρ_w decrease as a^{-4} [41] while ΔV remains almost constant, so in the regions where the false vacuum decays later, the total energy density becomes larger after a PT. Thus, the asynchronism of the vacuum decay process in different Hubble horizons induces superhorizon curvature perturbations. We notice that the uncertainty of the vacuum decay time is about β^{-1} at the length scale of β^{-1}, so that the equations of motion (3), (4), and (5) imply the corresponding amplitude of the energy density $\delta\rho(\beta^{-1})/\rho$ is approximately $\alpha\beta^{-1}$. Here, $\delta\rho(k^{-1})$ denotes the averaged density perturbation in a volume $\sim k^{-3}$, and $\alpha \equiv \Delta V/\rho_r(t_p)$ represents the strength of the PTs. Since the vacuum decay process becomes irrelevant at a length scale larger than β^{-1}, causality requires $\delta\rho(k^{-1})/\rho \propto k^{3/2}$ at the infrared region. [For $k^{-1} \gg \beta^{-1}$, the central-limit theorem implies the standard deviation $\sigma(k^{-1}) = \sigma(\beta^{-1})(\beta^{-1}k)^{3/2}$. This behavior is similar to that in Refs. [42,43], where the Poisson distribution of primordial black holes induces curvature perturbations with the power spectrum $\mathcal{P}_\mathcal{R}(k) \propto k^3$.] Then, the estimation of the standard deviation of $\delta\rho/\rho$ at the Hubble horizon scale can be described as

$$\delta_H \equiv \sqrt{(\delta\rho(H_*^{-1})/\rho)^2} \propto \alpha(\beta/H_*)^{-5/2}, \tag{6}$$

which is valid for $\alpha < 1$ and $\beta/H_* \gg 1$. The approximation (6) is then verified by numerical results of $\delta_H(\alpha, \beta/H_*)$ in the Supplemental Material [44], where we apply the postponed vacuum decay mechanism proposed in our previous work [24]. We find that δ_H is proportional to α for different values of β/H_*, and δ_H/α approaches the scaling relation $(\beta/H_*)^{-5/2}$ as in Eq. (6) for $\beta/H_* \gtrsim 10$.

The power spectrum of curvature perturbations, $\mathcal{P}_\mathcal{R}(k)$, is directly related to δ_H in the Press-Schechter formalism [45–47]

$$\delta_H^2 = \frac{16}{81}\int_0^\infty \frac{dk}{k}(kR_H)^4 W^2(k, R_H)\mathcal{P}_\mathcal{R}(k), \tag{7}$$

where $R_H = 1/(aH)$ is the comoving Hubble radius at the end of the PTs and we apply a Gaussian form window function [We choose the Gaussian type window function $W_{\rm GS}(k, R_H) = \exp(-k^2R_H^2)$ to strongly suppress the contribution from perturbations with $k > R_H^{-1}$, which is in accordance with the calculation of δ_H where we only take into account the delay of vacuum decay in the Hubble-sized regions and neglect the contribution from the smaller scales, $k \gtrsim R_H^{-1}$.] $W(k, R_H) = \exp(-k^2R_H^2)$. Since causality requires $\mathcal{P}_\mathcal{R}(k) \propto k^3$ for $k \ll \beta^{-1}$, we can obtain the approximate result of $\mathcal{P}_\mathcal{R}(k)$ in terms of the numerical results of $\delta_H(\alpha, \beta/H_*)$,

$$\mathcal{P}_\mathcal{R}(k) = 34.5\alpha^2[f(\beta/H_*)]^2(kR_H)^3, \tag{8}$$

where the constant 34.5 is obtained from Eq. (7). Since in the infrared regions $\mathcal{P}_\mathcal{R}(k) \propto k^3$, curvature perturbations induced during the PTs are much smaller than primordial perturbations from inflation at the CMB scales and do not affect the CMB observables.

Constraints on the PT parameters.—Since the PTs are expected to induce large curvature perturbations at small scales, the upper bounds on $\mathcal{P}_\mathcal{R}(k)$ can be converted into constraints on the PT parameters α, β/H_*, and T_*. The observations of CMB and large-scale structure give strict constraints on the power spectrum of curvature perturbations, $\mathcal{P}_\mathcal{R}(k) \sim 2 \times 10^{-9}$, at large scales $k \lesssim \mathcal{O}(1)$ Mpc^{-1}. At smaller scales, $\mathcal{P}_\mathcal{R}(k)$ is constrained by other observables, such as (i) the limits of the CMB spectral distortions, (ii) the helium abundance, (iii) the pulsar timing constraint

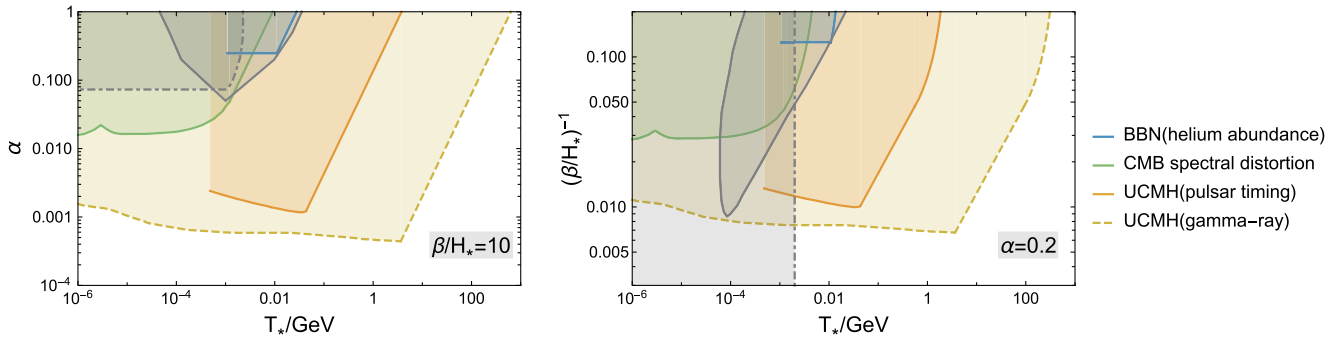

FIG. 1. The left and right panel show the constraint on α and β/H_* in the range $T_* \sim 10^{-6} - 10^3$ GeV, respectively, where we set $\beta/H_* = 10$ (left) and $\alpha = 0.2$ (right). The solid gray line and the dot-dashed gray line represent the current constraint from the upper bound of stochastic GW background [22] and big bang nucleosynthesis [60], respectively.

on the UCMH abundance, and (iv) the gamma-ray constraint on the UCMH abundance.

Setting the scale factor at present, $a_0 = 1$, in the radiation-dominated Universe, $R_H^{-1}/(10^4\ \mathrm{Mpc}^{-1}) \sim T_*/(1.1\ \mathrm{MeV})$, which roughly determines the range of T_* constrained by each upper bounds of $\mathcal{P}_\mathcal{R}(k)$. We set the cutoff of Eq. (8) at the Hubble horizon scale $k = R_H^{-1}$ to obtain a conservative estimation. In Fig. 1, we show the constraints on α and β/H_* in the range $T_* \sim 10^{-6} - 10^3$ GeV from each upper bounds of $\mathcal{P}_\mathcal{R}(k)$. The limit of CMB spectral distortions, including y distortion and μ distortion, implies $\mathcal{P}_\mathcal{R}(k) \lesssim 10^{-4}$ for the scales of $1\ \mathrm{Mpc}^{-1} \lesssim k \lesssim 10^4\ \mathrm{Mpc}^{-1}$ [48–50], which gives constraints on the PTs with $T_* < 1$ MeV, as shown in the green lines. In the range $10^4\ \mathrm{Mpc}^{-1} \lesssim k \lesssim 10^5\ \mathrm{Mpc}^{-1}$, $\mathcal{P}_\mathcal{R}(k)$ has to be smaller than 0.01 to avoid violating the BBN process and the prediction of primordial helium abundance [51–53]. The blue lines show the constraint from the observed helium abundance, constraining the PTs with $T_* \sim 1$–10 MeV. The authors of Refs. [54,55] find that UCMHs produce an observable period derivative of pulsars, and they apply the pulsar timing data to give the upper bound $\mathcal{P}_\mathcal{R}(k) \lesssim 10^{-6}$ for the scales of $4 \times 10^3\ \mathrm{Mpc}^{-1} \lesssim k \lesssim 4 \times 10^5\ \mathrm{Mpc}^{-1}$ setting the redshift of the UCMH collapse $z_c = 1000$ and detection threshold $s = 10$ ns. The orange lines show the constraint from the limit of UCMH abundance, constraining the PTs with $T_* \sim 0.3$ MeV $- 1$ GeV. The constraint presented in the dashed lines is from the nonobservation of gamma rays in UCMHs by the Fermi large area telescope, which applies in the case that WIMPs explain the nature of dark matter [56–59]. Here, we choose the mass of WIMP particles $m_\chi = 1$ TeV, the annihilation cross section $\langle\sigma v\rangle = 3 \times 10^{-26}\ \mathrm{cm}^3\ \mathrm{s}^{-1}$ and the UCMH redshift $z_c = 1000$ as in Fig. 6 of Ref. [56]. This upper bound imposes a very strong constraint on all PTs below 100 GeV. All the constraints above are evaluated at the 95% confidence level.

Since each of the constraint curves in Fig. 1 has a fairly flat bottom in a certain range, we can assume the constraints are irrelevant of T in those ranges and obtain the constraints in the $\alpha - \beta/H_*$ plane, as shown in Fig. 2. We obtain strict constraints on the QCD first-order PTs [32,61] (The standard QCD phase transition is crossover, but it becomes first order in the case of sufficiently large neutrino chemical potential [32].) and the low-scale dark PTs [62]. The constraint in this work is more strict on α than on β/H_*, as Eq. (8) implies. The most strict constraint on α is given by the limit of the UCMH abundance. In the case of $\beta/H_* \lesssim 10$, the parameter space $\alpha \gtrsim 2 \times 10^{-3}$ ($\alpha \gtrsim 6 \times 10^{-4}$) has been excluded model independently (model dependently) for $0.3\ \mathrm{MeV} \lesssim T_* \lesssim 100$ MeV ($T_* \lesssim 10$ GeV). Depending on the nature of dark matter, we also give the constraint on electroweak first-order PTs. In the case of $T_* = 100$ GeV, we obtain $\alpha \lesssim 0.1$ for $\beta/H_* = 10$ and $\beta/H_* \gtrsim 20$ for $\alpha = 0.2$, as shown in Fig. 1. As a comparison, the current constraint from the PTA experiments gives $\alpha \lesssim 0.1$ for $\beta/H_* = 10$ in the range $0.1\ \mathrm{MeV} \lesssim T_* \lesssim 0.1$ GeV at the 95% confidence level [21,22]. Reference [60] obtains $\alpha \lesssim \mathcal{O}(0.06)$ for the PTs after the BBN process ($T_* \lesssim 1$ MeV) since the decay products of false vacuum affects the prediction of BBN process. Compared to the previous constraints, this work gives a much more strict constraint on α in a larger range of

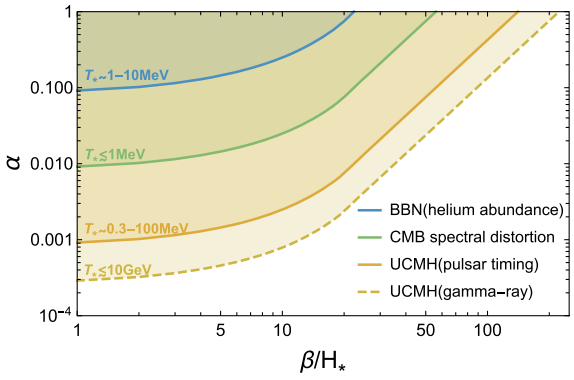

FIG. 2. The excluded parameter spaces of α and β/H_* obtained from each constraint on $\mathcal{P}_\mathcal{R}(k)$.

T_*. In the near future, the space-based GW detectors, such as LISA and *Taiji*, are sensitive to the PTs around the electroweak energy scale. If the future GW observables conflict with the model-dependent constraint (the dashed line shown in Figs. 1 and 2), the discovery of GWs from the PTs in turn gives constraints on the annihilation cross section of the dark matter models.

Conclusion and discussion.—We quantitatively investigate the superhorizon curvature perturbations induced by the first-order PTs, and for the first time give constraints on the PT parameters using various upper bounds of $\mathcal{P}_{\mathcal{R}}(k)$. The asynchronism of vacuum decay in different Hubble horizons induces large superhorizon curvature perturbations, which are then constrained by various observational results, such as the limits of the CMB spectral distortions, the helium abundance, and the UCMH abundance. This work gives strict constraints on α and β/H_* for the PT temperature below 100 GeV, including dark PTs, QCD first-order PTs and some electroweak first-order PTs. The result largely expands the currently excluded parameter spaces obtained from the nonobservation of the stochastic GW backgrounds, and give strict constraints especially on the low-temperature PTs and the slow PTs.

We have neglected the impact of thermal corrections on the PT dymanics [63–66] by assuming ΔV is a constant, the bubble velocity $v_{\rm w} \lesssim 1$ and energy transfer to the background plasma is instantaneous. Here, we qualitatively discuss how the thermal corrections affect the final result. The correction to ΔV may depend on T, but as long as ΔV decreases more slowly than $\rho_{\rm r}$ and $\rho_{\rm w}$, the constraints stay in the same order of magnitude. For the weak PTs, v_w tends to become smaller due to the friction of the background plasma. The superhorizon $\mathcal{P}_{\mathcal{R}}(k)$ is proportional to v_w^3 because the averaged bubble radius at the percolation time, $R_* \sim v_w/\beta$ and causality requires $\delta\rho(k^{-1})/\rho \sim k^{3/2}$. If the PT dynamics is feebly coupled to the plasma, the scalar field can oscillate in its quadratic potential for a long period and the energy density fraction of the scalar field increases with time. In this case, the induced $\mathcal{P}_{\mathcal{R}}(k)$ increases as $a^2(t)$ until the domination of the scalar field. Then, we have more strict constraints on the PT parameters, particularly for the PTs that happen at slightly higher temperatures.

In some inflationary models, for example, the ultra-slow-roll inflation [67], the small-scale $\mathcal{P}_{\mathcal{R}}$ is already very large before the PTs, induced curvature perturbations can become larger than the prediction of Eq. (8) as numerically studied in Ref. [68].

This work is supported in part by the National Key Research and Development Program of China Grants No. 2020YFC2201501, No. 2021YFC2203002, No. 2021YFC2203004 and No. 2021YFA0718304, in part by the National Natural Science Foundation of China Grants No. 11851302, No. 11947302, No. 11991052, No. 11821505, No. 12105060, No. 12105344 and No. 12075297, No. 12235019, No. 12147103, in part by the Science Research Grants from the China Manned Space Project with No. CMS-CSST-2021-B01, in part by the Fundamental Research Funds for the Central Universities. L. B. is supported by the National Natural Science Foundation of China under the Grants No. 12075041, No. 12147102, and the Fundamental Research Funds for the Central Universities of China (No. 2021CDJQY-011 and No. 2020CDJQY-Z003), and Chongqing Natural Science Foundation (Grants No. cstc2020jcyj-msxmX0814).

Note added.—We would like to acknowledge Ref. [69] which appeared recently. The authors also obtain similar constraints on the PT parameters from the CMB spectral distortions by considering the injected heat from the PTs into acoustic waves in the baryon-photon fluid.

*liujing@ucas.ac.cn
†lgbycl@cqu.edu.cn
‡cairg@itp.ac.cn
§guozk@itp.ac.cn
‖schwang@itp.ac.cn

[1] M. Losada, High temperature dimensional reduction of the MSSM and other multiscalar models in the limit, Phys. Rev. D **56**, 2893 (1997).
[2] J. M. Cline and P.-A. Lemieux, Electroweak phase transition in two Higgs doublet models, Phys. Rev. D **55**, 3873 (1997).
[3] M. Laine, Effective theories of MSSM at high temperature, Nucl. Phys. **B481**, 43 (1996); **B548**, 637(E) (1999).
[4] D. Bodeker, P. John, M. Laine, and M. G. Schmidt, The two loop MSSM finite temperature effective potential with stop condensation, Nucl. Phys. **B497**, 387 (1997).
[5] S. R. Coleman, The fate of the false vacuum. 1. Semiclassical theory, Phys. Rev. D **15**, 2929 (1977); **16**, 1248(E) (1977).
[6] C. G. Callan, Jr. and S. R. Coleman, The fate of the false vacuum. 2. First quantum corrections, Phys. Rev. D **16**, 1762 (1977).
[7] A. D. Linde, Fate of the false vacuum at finite temperature: Theory and applications, Phys. Lett. **100B**, 37 (1981).
[8] A. D. Linde, Decay of the false vacuum at finite temperature, Nucl. Phys. **B216**, 421 (1983); **B223**, 544(E) (1983).
[9] C. Caprini *et al.*, Science with the space-based interferometer eLISA. II: Gravitational waves from cosmological phase transitions, J. Cosmol. Astropart. Phys. 04 (2016) 001.
[10] C. Caprini *et al.*, Detecting gravitational waves from cosmological phase transitions with LISA: An update, J. Cosmol. Astropart. Phys. 03 (2020) 024.
[11] T. Vachaspati, Magnetic fields from cosmological phase transitions, Phys. Lett. B **265**, 258 (1991).
[12] Y. Di, J. Wang, R. Zhou, L. Bian, R.-G. Cai, and J. Liu, Magnetic Field and Gravitational Waves from the First-Order Phase Transition, Phys. Rev. Lett. **126**, 251102 (2021).

[13] J. Yang and L. Bian, Magnetic field generation from bubble collisions during first-order phase transition, Phys. Rev. D **106**, 023510 (2022).

[14] D. E. Morrissey and M. J. Ramsey-Musolf, Electroweak baryogenesis, New J. Phys. **14**, 125003 (2012).

[15] M. D'Onofrio, K. Rummukainen, and A. Tranberg, Sphaleron Rate in the Minimal Standard Model, Phys. Rev. Lett. **113**, 141602 (2014).

[16] P. Amaro-Seoane *et al.* (LISA Collaboration), Laser interferometer space antenna, arXiv:1702.00786.

[17] W.-H. Ruan, Z.-K. Guo, R.-G. Cai, and Y.-Z. Zhang, Taiji program: Gravitational-wave sources, Int. J. Mod. Phys. A **35**, 2050075 (2020).

[18] J. Luo *et al.* (TianQin Collaboration), TianQin: A space-borne gravitational wave detector, Classical Quantum Gravity **33**, 035010 (2016).

[19] J. Aasi *et al.* (LIGO Scientific Collaboration), Advanced LIGO, Classical Quantum Gravity **32**, 074001 (2015).

[20] C. L. Carilli and S. Rawlings, Science with the square kilometer array: Motivation, key science projects, standards and assumptions, New Astron. Rev. **48**, 979 (2004).

[21] Z. Arzoumanian *et al.* (NANOGrav Collaboration), Searching for Gravitational Waves from Cosmological Phase Transitions with the NANOGrav 12.5-Year Dataset, Phys. Rev. Lett. **127**, 251302 (2021).

[22] X. Xue *et al.*, Constraining Cosmological Phase Transitions with the Parkes Pulsar Timing Array, Phys. Rev. Lett. **127**, 251303 (2021).

[23] A. Romero, K. Martinovic, T. A. Callister, H.-K. Guo, M. Martínez, M. Sakellariadou, F.-W. Yang, and Y. Zhao, Implications for First-Order Cosmological Phase Transitions from the Third LIGO-Virgo Observing Run, Phys. Rev. Lett. **126**, 151301 (2021).

[24] J. Liu, L. Bian, R.-G. Cai, Z.-K. Guo, and S.-J. Wang, Primordial black hole production during first-order phase transitions, Phys. Rev. D **105**, L021303 (2022).

[25] A. H. Guth and E. J. Weinberg, Could the universe have recovered from a slow first order phase transition?, Nucl. Phys. **B212**, 321 (1983).

[26] E. J. Weinberg, Some problems with extended inflation, Phys. Rev. D **40**, 3950 (1989).

[27] A. R. Liddle and D. Wands, Hyperextended inflation: Dynamics and constraints, Phys. Rev. D **45**, 2665 (1992).

[28] A. R. Liddle and D. Wands, Microwave background constraints on extended inflation voids, Mon. Not. R. Astron. Soc. **253**, 637 (1991).

[29] M. S. Turner, E. J. Weinberg, and L. M. Widrow, Bubble nucleation in first order inflation and other cosmological phase transitions, Phys. Rev. D **46**, 2384 (1992).

[30] E. J. Copeland, A. R. Liddle, D. H. Lyth, E. D. Stewart, and D. Wands, False vacuum inflation with Einstein gravity, Phys. Rev. D **49**, 6410 (1994).

[31] N. Aghanim *et al.* (Planck Collaboration), Planck 2018 results. VI. Cosmological parameters, Astron. Astrophys. **641**, A6 (2020); **652**, C4(E) (2021).

[32] D. J. Schwarz and M. Stuke, Lepton asymmetry and the cosmic QCD transition, J. Cosmol. Astropart. Phys. 11 (2009) 025; 10 (2010) E01.

[33] P. Schwaller, Gravitational Waves from a Dark Phase Transition, Phys. Rev. Lett. **115**, 181101 (2015).

[34] J. M. Cline and K. Kainulainen, Electroweak baryogenesis and dark matter from a singlet Higgs, J. Cosmol. Astropart. Phys. 01 (2013) 012.

[35] M. Jiang, L. Bian, W. Huang, and J. Shu, Impact of a complex singlet: Electroweak baryogenesis and dark matter, Phys. Rev. D **93**, 065032 (2016).

[36] M. Chala, G. Nardini, and I. Sobolev, Unified explanation for dark matter and electroweak baryogenesis with direct detection and gravitational wave signatures, Phys. Rev. D **94**, 055006 (2016).

[37] A. Beniwal, M. Lewicki, J. D. Wells, M. White, and A. G. Williams, Gravitational wave, collider and dark matter signals from a scalar singlet electroweak baryogenesis, J. High Energy Phys. 08 (2017) 108.

[38] R. Emami and G. Smoot, Observational constraints on the primordial curvature power spectrum, J. Cosmol. Astropart. Phys. 01 (2018) 007.

[39] A. D. Gow, C. T. Byrnes, P. S. Cole, and S. Young, The power spectrum on small scales: Robust constraints and comparing PBH methodologies, J. Cosmol. Astropart. Phys. 02 (2021) 002.

[40] K. Enqvist, J. Ignatius, K. Kajantie, and K. Rummukainen, Nucleation and bubble growth in a first order cosmological electroweak phase transition, Phys. Rev. D **45**, 3415 (1992).

[41] W. H. Press, B. S. Ryden, and D. N. Spergel, Dynamical evolution of domain walls in an expanding universe, Astrophys. J. **347**, 590 (1989).

[42] T. Papanikolaou, V. Vennin, and D. Langlois, Gravitational waves from a universe filled with primordial black holes, J. Cosmol. Astropart. Phys. 03 (2021) 053.

[43] N. Afshordi, P. McDonald, and D. N. Spergel, Primordial black holes as dark matter: The power spectrum and evaporation of early structures, Astrophys. J. Lett. **594**, L71 (2003).

[44] See Supplemental Material at http://link.aps.org/supplemental/10.1103/PhysRevLett.130.051001 for the details of the postponed vacuum decay mechanism and the numerical results of $\delta_H(\alpha, \beta/H_*)$.

[45] W. H. Press and P. Schechter, Formation of galaxies and clusters of galaxies by self-similar gravitational condensation, Astrophys. J. **187**, 425 (1974).

[46] K. Ando, K. Inomata, and M. Kawasaki, Primordial black holes and uncertainties in the choice of the window function, Phys. Rev. D **97**, 103528 (2018).

[47] C.-M. Yoo, T. Harada, J. Garriga, and K. Kohri, Primordial black hole abundance from random Gaussian curvature perturbations and a local density threshold, Prog. Theor. Exp. Phys. **2018**, 123E01 (2018).

[48] J. Chluba, A. L. Erickcek, and I. Ben-Dayan, Probing the inflaton: Small-scale power spectrum constraints from measurements of the CMB energy spectrum, Astrophys. J. **758**, 76 (2012).

[49] J. Chluba, J. Hamann, and S. P. Patil, Features and new physical scales in primordial observables: Theory and observation, Int. J. Mod. Phys. D **24**, 1530023 (2015).

[50] M. Lucca, N. Schöneberg, D. C. Hooper, J. Lesgourgues, and J. Chluba, The synergy between CMB spectral distortions and anisotropies, J. Cosmol. Astropart. Phys. 02 (2020) 026.

[51] D. Jeong, J. Pradler, J. Chluba, and M. Kamionkowski, Silk Damping at a Redshift of a Billion: A New Limit on Small-Scale Adiabatic Perturbations, Phys. Rev. Lett. **113**, 061301 (2014).
[52] T. Nakama, T. Suyama, and J. Yokoyama, Reheating the Universe Once More: The Dissipation of Acoustic Waves as a Novel Probe of Primordial Inhomogeneities on Even Smaller Scales, Phys. Rev. Lett. **113**, 061302 (2014).
[53] K. Inomata, M. Kawasaki, and Y. Tada, Revisiting constraints on small scale perturbations from big-bang nucleosynthesis, Phys. Rev. D **94**, 043527 (2016).
[54] H. A. Clark, G. F. Lewis, and P. Scott, Investigating dark matter substructure with pulsar timing—I. Constraints on ultracompact minihaloes, Mon. Not. R. Astron. Soc. **456**, 1394 (2016); **464**, 2468(E) (2017).
[55] H. A. Clark, G. F. Lewis, and P. Scott, Investigating dark matter substructure with pulsar timing—II. Improved limits on small-scale cosmology, Mon. Not. R. Astron. Soc. **456**, 1402 (2016); **464**, 955(E) (2017).
[56] T. Bringmann, P. Scott, and Y. Akrami, Improved constraints on the primordial power spectrum at small scales from ultracompact minihalos, Phys. Rev. D **85**, 125027 (2012).
[57] T. Nakama, T. Suyama, K. Kohri, and N. Hiroshima, Constraints on small-scale primordial power by annihilation signals from extragalactic dark matter minihalos, Phys. Rev. D **97**, 023539 (2018).
[58] M. Kawasaki, H. Nakatsuka, and K. Nakayama, Constraints on small-scale primordial density fluctuation from cosmic microwave background through dark matter annihilation, J. Cosmol. Astropart. Phys. 03 (2022) 061.
[59] M. S. Delos, A. L. Erickcek, A. P. Bailey, and M. A. Alvarez, Density profiles of ultracompact minihalos: Implications for constraining the primordial power spectrum, Phys. Rev. D **98**, 063527 (2018).
[60] Y. Bai and M. Korwar, Cosmological constraints on first-order phase transitions, Phys. Rev. D **105**, 095015 (2022).
[61] F. Gao and I. M. Oldengott, Cosmology Meets Functional QCD: First-Order Cosmic QCD Transition Induced by Large Lepton Asymmetries, Phys. Rev. Lett. **128**, 131301 (2022).
[62] M. Breitbach, J. Kopp, E. Madge, T. Opferkuch, and P. Schwaller, Dark, cold, and noisy: Constraining secluded hidden sectors with gravitational waves, J. Cosmol. Astropart. Phys. 07 (2019) 007.
[63] J. Ellis, M. Lewicki, and J. M. No, On the maximal strength of a first-order electroweak phase transition and its gravitational wave signal, J. Cosmol. Astropart. Phys. 04 (2019) 003.
[64] J. R. Espinosa, T. Konstandin, J. M. No, and G. Servant, Energy budget of cosmological first-order phase transitions, J. Cosmol. Astropart. Phys. 06 (2010) 028.
[65] W.-Y. Ai, B. Garbrecht, and C. Tamarit, Bubble wall velocities in local equilibrium, J. Cosmol. Astropart. Phys. 03 (2022) 015.
[66] M. Lewicki, M. Merchand, and M. Zych, Electroweak bubble wall expansion: Gravitational waves and baryogenesis in Standard Model-like thermal plasma, J. High Energy Phys. 02 (2022) 017.
[67] J. Garcia-Bellido and E. Ruiz Morales, Primordial black holes from single field models of inflation, Phys. Dark Universe **18**, 47 (2017).
[68] R. Jinno, T. Konstandin, H. Rubira, and J. van de Vis, Effect of density fluctuations on gravitational wave production in first-order phase transitions, J. Cosmol. Astropart. Phys. 12 (2021) 019.
[69] N. Ramberg, W. Ratzinger, and P. Schwaller, One μ to rule them all: CMB spectral distortions can probe domain walls, cosmic strings and low scale phase transitions, arXiv:2209.14313.